Photoreaction channels of the guanine–cytosine base pair explored by long-range corrected TDDFT calculations†

Shohei Yamazaki* and Tetsuya Taketsugu

Department of Chemistry, Faculty of Science, Hokkaido University, Sapporo 060-0810, Japan.

E-mail: shohei@mail.sci.hokudai.ac.jp

† Electronic supplementary information (ESI) available: vertical excitation energies calculated with basis sets of double-zeta plus polarization quality, and additional figures of potential energy profiles.

Abstract

Photoinduced processes in the Watson–Crick guanine–cytosine base pair are comprehensively studied by means of long-range corrected (LC) TDDFT calculations of potential energy profiles using the LC-BLYP and CAM-B3LYP functionals. The ab initio CC2 method and the conventional TDDFT method with the B3LYP functional are also employed to assess the reliability of the LC-TDDFT method. The present approach allows us to compare the potential energy profiles at the same computational level for excited-state reactions of the base pair, including single and double proton transfer between the bases and nonradiative decay via ring puckering in each base. In particular, long-range correction to the TDDFT method is critical for a qualitatively correct description of the proton transfer reactions. The calculated energy profiles exhibit low barriers for out-of-plane deformation of the guanine moiety in the locally-excited state, which is expected to lead to a conical intersection with the ground state, as well as for single proton transfer from guanine to cytosine with the well-known electron-driven proton transfer mechanism. Thus the present results suggest that both processes can compete in hydrogen-bonded base pairs and play a significant role in the mechanism of photostability.

1. Introduction

Photophysics and photochemistry of nucleic acid bases and base pairs have been extensively studied for understanding the mechanism of the photostability and photodamage in DNA.[1,2] For individual bases, ultrafast nonradiative decay via a conical intersection (CI) between electronic ground and excited states[3] is well recognized as the mechanism of photostability which prevents destructive photoreations by extremely shortening the lifetime of the excited state. For base pairs, it has been revealed that hydrogen bonds between the monomer bases play significant roles in the photoinduced processes. One of the most important photoreactions induced by interbase hydrogen bonding is so-called electron-driven proton transfer (EDPT), i.e. intermolecular single proton transfer (SPT) in the excited state following the transition to a charge-transfer (CT) state. Sobolewski, Domcke and co-workers[4-8] proposed that the EDPT reaction provides an efficient mechanism of nonradiative decay via CIs which is unique to hydrogen-bonded base pairs. Another important photoreaction is double proton transfer (DPT) between the bases, which was suggested as a potential mechanism of photoinduced mutation in DNA.[9,10] Nonradiative deactivation of bases and base pairs in DNA environment has also been an important subject of theoretical studies.[11-15] In spectroscopic experiments, the effect of hydrogen bonding on the excited-state lifetime of the base pairs has been of great interest.[16-26]

In the present work, excited-state potential energy profiles of the Watson–Crick form of the guanine–cytosine (GC) base pair are theoretically studied for all of the potentially competing reactions mentioned above: SPT and DPT between guanine (G) and cytosine (C) as well as nonradiative decay in each single base under hydrogen bonding. One purpose of this study is to assess the favorability of the decay process in the G monomer with hydrogen-bonded to C, which was rarely discussed in previous studies. In the case of individual bases without hydrogen bonding, potential energy profiles of the nonradiative decay via CIs have been studied by many groups for both G[27-30] and C.[31-37] For the GC pair, Guallar et al.[10] studied the excited-state potential energy profiles of the DPT reaction, while Sobolewski, Domcke and co-workers[5,7] proposed the SPT reaction from G to C with the EDPT mechanism and nonradiative decay

process of C in hydrogen bonding. Further theoretical studies have been carried out for the EDPT reaction in the gas phase, solution and DNA environment.[11,14,38] However, potential energy profiles for the decay path of G in hydrogen bonding were not calculated, presumably because this decay process, accompanying a large out-of-plane distortion of the six-membered ring and amino group in G, seems to be strongly suppressed by the hydrogen bonds with C at a glance.

Another purpose of the present work is to compare the favorability of the possible photoreactions in the GC pair. Potential energy profiles of each process (except the decay in G under hydrogen bonding) have been studied individually, but a comprehensive theoretical study comparing all possible reactions is still missing. Therefore, it remains not fully understood which photoreaction is the most likely to occur.

For the two purposes above, we apply the long-range corrected time-dependent density functional theory (LC-TDDFT) method[39,40] for the calculation of excited-state potential energy curves. The advantage of using this method is that the potential energy profiles of possible photoinduced processes can be compared at the same computational level. The TDDFT method may be problematic for describing potential energy surfaces near a CI, because this is a single-reference method. However, the barrier on the excited-state reaction path, which is a crucial factor determining the favorability of each photoinduced process including nonradiative decay via a CI, is expected to be accurately calculated at the TDDFT level due to the inclusion of dynamic electron correlation to a certain extent.

More importantly, the long-range correction (LC) to TDDFT is critical for a correct description of the potential energy curves in the CT state, which is a key state for the EDPT reaction of base pairs. It is well known that conventional density functionals without LC extremely underestimate the CT excitation energies of base pairs.[4,41-45] The LC-TDDFT method can avoid this problem by introducing the Hartree-Fock exchange integral for long interelectronic distance.[42-45] It is noteworthy that in our previous study the LC-TDDFT method qualitatively reproduced the results of the ab initio complete-active-space second-order perturbation theory (CASPT2) calculation for the potential energy curves along the excited-state DPT reaction path in the hydrogen-bonded dimer of 7-azaindole (7AI).[45] In the present

work, the TDDFT results are compared with ab initio results using the approximate second-order coupled-cluster singles-and-doubles (CC2) method.[46]

The organization of this paper is as follows: Section 2 gives details of the computational methods applied in the present work. Section 3.1 shows vertical excitation energies calculated at the TDDFT and CC2 levels. Sections 3.2 and 3.3 discuss the potential energy profiles for the decay path of the G moiety and other reaction paths, respectively. Conclusions are given in Section 4.

2. Computational methods

The present work applied two long-range corrected functionals for the DFT and TDDFT calculations of the GC pair. One is the Becke 1988 exchange[47] + Lee–Yang–Parr correlation[48] functional augmented by the LC scheme (LC-BLYP functional), and the other is a long-range corrected version of the B3LYP functional using the Coulomb-attenuating method (CAM-B3LYP functional).[49] The conventional B3LYP functional[50,51] was also applied for some calculations in order to assess the effect of long-range correction on the excited-state potential energy profiles. The Sapporo-DZP and Sapporo-TZP basis sets by Noro et al.[52] were employed, hereafter denoted as DZP and TZP, respectively. The (TD)DFT calculations were carried out using the GAMESS program package.[53]

Ground-state equilibrium geometry was determined at the LC-BLYP level with the DZP basis set. Vertical excitation energies at the optimized geometry were calculated with the TDDFT method using the LC-BLYP, CAM-B3LYP and B3LYP functionals (TD-LC-BLYP, TD-CAM-B3LYP and TD-B3LYP methods, respectively) and the DZP and TZP basis sets. Geometries of the excited-state stationary points including minima and transition states were optimized at the TD-LC-BLYP/DZP level, and also at the TD-CAM-B3LYP/DZP level for selected structures. No symmetry constraint was imposed during the optimization if not specified. Normal mode analysis was also performed for each

stationary point in the ground and excited states. The energies of the excited-state stationary points were recalculated using each functional with the TZP basis set.

The intrinsic reaction coordinate (IRC) calculation at the TD-LC-BLYP/DZP level was carried out starting with each transition-state structure in the excited state. For some of the calculated IRC paths, potential energy curves of the ground state and low-lying excited states were calculated at the TD-LC-BLYP/DZP level as well as the TD-CAM-B3LYP/DZP and TD-B3LYP/DZP levels.

To check the accuracy of the present TDDFT results, the CC2 method with the resolution-of-identity (RI) approximation[46,54] was also applied for some energy calculations. The def2-SV(P) and def2-TZVP basis sets by Ahlrichs and co-workers[55-57] were employed, hereafter denoted as SV(P) and TZVP, respectively. The CC2 calculations were performed with TURBOMOLE 6.3.[58]

3. Results and discussion

3.1. Vertical excitation energies

The equilibrium geometry of the GC pair in the S_0 state determined at the LC-BLYP/DZP level is a planar structure in C_s symmetry, which is confirmed by normal mode analysis. Table 1 shows the vertical excitation energies (ΔE) and oscillator strengths (f) of the lowest 10 singlet excited states calculated at this Franck–Condon (FC) geometry. The TDDFT/TZP method with the LC-BLYP, CAM-B3LYP and B3LYP functionals as well as the CC2/TZVP method is employed for the calculation. The table also includes the results for isolated monomers of G and C, which are calculated at the S_0 geometry of each base optimized with the LC-BLYP/DZP method in C_s symmetry. The corresponding TDDFT and CC2 results with the DZP and SV(P) basis sets, respectively, are given in the ESI. The TDDFT/DZP excitation energies with each functional differ by less than 0.1 eV from the respective TZP values for the $^1\pi\pi^*$ and $^1n\pi^*$ states. The CC2/SV(P) results qualitatively agree with the CC2/TZVP ones, where the former energies are about 0.2–0.3 eV higher than the latter for each state.

At the TD-LC-BLYP/TZP level, the vertical excitation energies of the lowest two excited states for the FC geometry are 5.09 and 5.27 eV, respectively, and the oscillator strengths of these states are 0.080 and 0.113; see Table 1. The S_1 and S_2 states are locally-excited (LE) states characterized by the $^1\pi\pi^*$ excitation in the G and C moieties, respectively, labeled as $^1\pi\pi^*$ (G → G*) and $^1\pi\pi^*$ (C → C*). The S_3 state is another $^1\pi\pi^*$ (G → G*) state, which exhibits the vertical excitation energy of 5.68 eV and oscillator strength of 0.465. The first and second $^1\pi\pi^*$ (G → G*) states are of the ^1L_a and ^1L_b characters, respectively, the former of which is dominated by the excitation from the highest occupied molecular orbital (HOMO) to the lowest unoccupied molecular orbital (LUMO) of G and the latter is from HOMO to LUMO+1 of G. The ^1L_a and ^1L_b characters are also observed for the lowest two $^1\pi\pi^*$ states of the isolated G monomer shown in Table 1, which agrees with the CASPT2 results by Fülscher et al.[59] These findings about the excitation energies and oscillator strengths of the GC pair are consistent with the absorption spectrum of the heterodimer of guanosine and cytidine in solution,[24] where the bands for the lowest $^1\pi\pi^*$ (G → G*) and $^1\pi\pi^*$ (C → C*) states are at ~280 nm and the band for the second $^1\pi\pi^*$ (G → G*) state at ~250 nm exhibits more intense peak.

For the lowest three LE states, the TD-CAM-B3LYP and TD-B3LYP results are consistent with the TD-LC-BLYP ones with respect to the excitation energies and oscillator strengths, as shown in Table 1. The CC2 calculations reproduce the TDDFT results for these states. In particular, they predict that the S_1 and S_2 states are the lowest $^1\pi\pi^*$ (G → G*) and $^1\pi\pi^*$ (C → C*) states, respectively. The CC2/TZVP vertical excitation energies of these states are 4.88 and 5.06 eV, and the oscillator strengths are 0.061 and 0.063. The second $^1\pi\pi^*$ (G → G*) state exhibits the excitation energy of 5.51 eV and oscillator strength of 0.425.

The lowest CT state of the GC pair is represented by the charge transfer from a π orbital of G to a π* orbital of C in the TDDFT and CC2 calculations. This excitation is labeled as $^1\pi\pi^*$ (G → C*). The TD-LC-BLYP/TZP vertical excitation energy of the lowest $^1\pi\pi^*$ (G → C*) state, appearing as the S_7 state, is calculated to be 6.00 eV (see Table 1). The oscillator strength for this state is 0.008. At the CC2/TZVP

level, the lowest $^1\pi\pi^*$ (G → C*) state is the S_3 state, whose excitation energy is 5.23 eV. These results suggest that the LC-BLYP functional tends to overestimate the excitation energy of CT states compared to the CC2 method. On the other hand, the CAM-B3LYP functional underestimates the CT excitation energy. The TD-CAM-B3LYP/TZP excitation energy of the lowest $^1\pi\pi^*$ (G → C*) state is calculated to be 4.93 eV, which is lower than the energy of the LE states. The difference between the LC-BLYP and CAM-B3LYP functionals reflects the extent of long-range correction: The former uses 100% of the Hartree-Fock exchange in the limit of the infinitely long interelectronic distance, while the latter uses less than 100% even in this limit (65% in the present calculation). The B3LYP functional drastically underestimates the CT excitation energy because of the lack of LC. As a result, there appear three CT states below the lowest LE state at the TD-B3LYP/TZP level, including the $^1\pi\pi^*$ (G → C*) and $^1n\pi^*$ (G → C*) excitations. These findings in the TDDFT and CC2 calculations are consistent with previous theoretical studies.[5,43,44]

The $^1\pi\pi^*$ (G → G*) states of the GC pair exhibit slightly lower excitation energy than the corresponding $^1\pi\pi^*$ states of the isolated G monomer, while the $^1\pi\pi^*$ (C → C*) states exhibit higher energy than those of the isolated C monomer; see Table 1. For the $^1n\pi^*$ states, the excitation energy of the GC pair is blue-shifted compared with the G and C isolated monomers. This is because the hydrogen bonds to the oxygen (O) atoms of G and C and to the nitrogen (N) atom of C increases the energy for the excitation from the lone-pair orbitals on these atoms. Some $^1\pi\sigma^*$ states appear in higher excited states of the GC pair and G monomer, but the present results for these states are less reliable. Correct description of the $^1\pi\sigma^*$ state requires diffuse functions for the basis set, because this state is of a Rydberg character in the FC region. Although the TD-B3LYP method exhibits particularly low energies of the $^1\pi\sigma^*$ state (see Table 1), this is a result of the underestimation of the Rydberg excitation energy by the conventional functional lacking LC.

In the following sections, we focus on the photoinduced processes after the excitation to the lowest $^1\pi\pi^*$ (G → G*) and $^1\pi\pi^*$ (C → C*) states. These states are relabeled as the LE (G → G*) and

LE (C → C*) states, respectively, to emphasize the LE character. The lowest $^1\pi\pi^*$ (G → C*) state is renamed as the CT (G → C*) state for the same reason. We use the LC-BLYP functional for the excited-state geometry optimization at the TDDFT level in most cases. This is because the TD-LC-BLYP method reproduces the ab initio result that the first and second LE states are lower in energy than the first CT state, while the TD-CAM-B3LYP and TD-B3LYP methods do not reproduce this result. The energetic order of the LE and CT states would be a critical factor to determine what reaction mechanism is likely in the photoexcited GC pair. The TD-CAM-B3LYP method is also used for the optimization in some cases, to assess the effect of the extent of LC on the potential energy profiles.

3.2. Decay channel of guanine with hydrogen-bonded to cytosine

Fig. 1 shows the TD-LC-BLYP/TZP energy diagram for the presently studied photoreactions in the GC pair, where the stationary-point geometries are optimized at the (TD-)LC-BLYP/DZP level. Geometry optimization of the LE (G → G*) state in C_1 symmetry starting near the FC region leads to a minimum of non-planar structure on the S_1 potential energy surface, which is labeled as MIN_{LE1}. This minimum is 4.70 eV higher in energy than the FC geometry. When the optimization is performed with C_s symmetry constraint, the resulting structure is found to be a second-order saddle point which has two imaginary-frequency modes corresponding to out-of-plane motion. This structure is denoted as SP_{LE1}. The energy of this saddle point is higher by 4.90 eV than the S_0 minimum energy.

Excited-state potential energy profiles were calculated for the reaction paths from MIN_{LE1}. As shown in Fig. 1, the considered processes include nonradiative decay in G with hydrogen-bonded to C, SPT reaction via the EDPT mechanism (from G to C and from C to G), DPT reaction between the bases, and nonradiative decay in C with hydrogen-bonded to G following the transition to the LE (C → C*) state. The decay process in C is also likely to occur after the LE (C → C*) excitation at the FC geometry by a relaxation from the S_2 to S_1 state through a barrierless pathway. This is expected because of the result that geometry optimization of the S_2 state starting in the FC region leads to a minimum of a planar

structure representing an avoided crossing with the S_1 state, which exhibits the energy difference of about 0.1 eV between the S_1 and S_2 states and mixing of the configurations for the LE (G → G*) and LE (C → C*) excitations. The rest of this section focuses on the decay path in the G moiety, while other paths are discussed in Section 3.3.

For the nonradiative decay of G in the GC pair, the IRC path in the S_1 state from MIN_{LE1} exhibits an intermediate minimum, denoted as MIN_{LE2}, and two transition states, labeled as $TS_{LE1\text{-}LE2}$ and $TS_{LE2\text{-}LE3}$; see Fig. 1. The S_1 state is of the LE (G → G*) character all along the IRC path. The barrier height at $TS_{LE1\text{-}LE2}$ and $TS_{LE2\text{-}LE3}$ is 0.11 and 0.17 eV, respectively, from MIN_{LE1}. The energy of $TS_{LE2\text{-}LE3}$ is 0.07 eV higher than that of MIN_{LE2}. For both transition states, the potential energy (4.81 and 4.87 eV at $TS_{LE1\text{-}LE2}$ and $TS_{LE2\text{-}LE3}$, respectively, relative to the S_0 minimum energy) is lower than the vertical excitation energy of the LE (G → G*) state at the FC geometry (5.09 eV). This result suggests that the decay path through these transition states is energetically accessible after UV absorption.

The IRC path finally reaches another minimum in the LE (G → G*) state, referred to as MIN_{LE3}. This minimum exhibits a significant out-of-plane deformation of the six-membered ring and amino group. Similar deformation is observed for CI structure of the isolated monomer of G.[27-30] The energy of MIN_{LE3} is 4.58 eV relative to the S_0 minimum energy, which is considerably lower than the vertical excitation energy and the energy of MIN_{LE1}. In addition, the energy gap between the LE (G → G*) and S_0 states is reduced to 1.1 eV at MIN_{LE3}, and an S_1–S_0 CI is expected to be reached by additional deformation from there (see the ESI). These results suggest that efficient nonradiative decay of G via a CI is likely to occur even in the GC pair. It should be noted that the energy of the S_1–S_0 crossing shown in the ESI may be overestimated (about 0.4 eV higher than MIN_{LE3} at the TD-LC-BLYP/DZP level), because of the computational limitation that geometry optimization for the minimum energy point of crossing could not be performed with the present method. The energy of crossing would be likely much lower if the optimization could be done. It might also be possible that the IRC path directly reaches the S_1–S_0 CI without MIN_{LE3} being found if it is calculated with a multi-reference method such as MRCI (multi-reference configuration interaction).

Fig. 2 shows in detail the TD-LC-BLYP/DZP-optimized geometry of excited-state stationary points relevant to the out-of-plane deformation of the G moiety in the GC pair. At MIN_{LE1}, the out-of-plane deformation of the six-membered ring is characterized by a pyramidalization at the N1 and C4 atoms of G (see Fig. 2a for the structure and atom labeling). This finding is consistent with the excited-state minimum located by configuration interaction singles (CIS) calculations.[5] In the first step of deformation, namely, from MIN_{LE1} to MIN_{LE2}, the pyramidalization is enhanced at the N1 atom, while largely reduced at the C4 atom. As a result, the dihedral angle δ(N1-C2-N3-C4), which represents the twisting of C2=N3 double bond, is about 60 degrees larger at MIN_{LE2} than at MIN_{LE1}. In the second step, namely, from MIN_{LE2} to MIN_{LE3}, out-of-plane distortion of the amino group of G is significantly enhanced by the pyramidalization at the C2 atom. The dihedral angle δ(C4-N3-C2-N10) representing this distortion is −145.6° and −75.9° at MIN_{LE2} and MIN_{LE3}, respectively. The large twisting of the C=N double bond and distortion of the amino group are well known as characteristic feature of CI structure in a single base of G.[27-30]

The lengths of the three interbase hydrogen bonds at MIN_{LE1}, between the O atom of G and the hydrogen (H) atom of C, between the H atom of G and the N atom of C, and between the H atom of G and the O atom of C, are 1.593, 1.805, and 1.740 Å, respectively (see Fig. 2a). These bonds become longer by about 0.1–0.2 Å at the other stationary points shown in Fig. 2, implying weaker hydrogen-bond strength between G and C. Thus it is expected that the energy of MIN_{LE1} is more stabilized than other out-of-plane deformed structures by the stronger hydrogen-bond interaction.

For the isolated monomer of G, any minima corresponding to MIN_{LE1}, MIN_{LE2} or MIN_{LE3} could not be located by geometry optimization in the $^1\pi\pi^*$ state with the TD-LC-BLYP/DZP method. All attempts of the optimization led to a crossing with the ground state, where the molecular structure exhibits a significant out-of-plane deformation of the six-membered ring and is similar to the geometry of CI reported in previous theoretical studies.[27-30] Thus the present TDDFT calculations predict that the nonradiative decay path of the isolated G is barrierless. Such a decay path of G with no barrier was also predicted by CASPT2 calculations of the potential energy profiles.[27,29,30] The consistency between the

DFT and ab initio results supports the conclusion that the appearance of MIN_{LE1} in the GC pair is likely due to the stabilization by hydrogen bonding between the bases and not a computational artifact of the TDDFT calculation.

To further support the existence of barriers on the decay channel in hydrogen-bonded G, the stationary-point energies along the reaction path from MIN_{LE1} to MIN_{LE3} were calculated with different computational methods. Table 2 gives the resulting energies of the S_1 state with LE (G → G*) character, which are relative to the S_0 minimum energy. Each method predicts low energy barriers with the height of less than 0.2 eV (from MIN_{LE1}) at the two transition-state structures, ensuring the accessibility of this decay path after the excitation to the LE (G → G*) state.

As shown in the upper half of Table 2, the TD-LC-BLYP and CC2 methods were applied for the single-point energy calculations of the minimum and transition-state structures optimized at the TD-LC-BLYP/DZP level. In the energy calculations with the TD-LC-BLYP method, the TZP and DZP basis sets give very similar results. The difference between the energies with the two basis sets is less than 0.1 eV at each structure. It should be noticed that both basis sets predict the two barriers at transition-state structures. At the TD-LC-BLYP/DZP level, the barrier height of $TS_{LE1\text{-}LE2}$ and $TS_{LE2\text{-}LE3}$ from MIN_{LE1} is 0.06 and 0.07 eV, respectively, and the latter exhibits 0.04 eV higher energy than MIN_{LE2}. For MIN_{LE3}, the TD-LC-BLYP/DZP method gives the energy gap of 1.0 eV between the S_1 and S_0 states.

The CC2 calculation also supports the existence of the two barriers. For the first step from MIN_{LE1} to MIN_{LE2}, the barrier height is estimated to be 0.05 and 0.08 eV at the CC2/TZVP and CC2/SV(P) levels, respectively. Note that the energy of this barrier is calculated for the highest-energy point at the CC2/SV(P) level along the IRC path between the TD-LC-BLYP/DZP-optimized structures of MIN_{LE1} and $TS_{LE1\text{-}LE2}$, because the CC2 energy of the $TS_{LE1\text{-}LE2}$ structure was calculated to be lower than that of MIN_{LE1}. For the second step from MIN_{LE2} to MIN_{LE3}, the CC2 barrier height is calculated at the $TS_{LE2\text{-}LE3}$ structure. The barrier exhibits higher energy by 0.10 and 0.07 eV than MIN_{LE2} at the CC2/TZVP and CC2/SV(P) levels, respectively, while it exhibits slightly lower energy than MIN_{LE1}. For each structure, the CC2 method gives lower energy than the TD-LC-BLYP method, and the CC2/TZVP

energy is lower than the CC2/SV(P) energy by about 0.2 eV or less. The S_1–S_0 energy gap of MIN_{LE3} is calculated to be about 0.8 eV at the CC2 level with each basis set.

Geometry optimization at the TD-CAM-B3LYP/DZP level was also performed for the stationary-point structures corresponding to those in Fig. 2. The single-point energies of the resulting structures were calculated at the TD-CAM-B3LYP and CC2 levels; see the lower half of Table 2. One can see that both methods support the existence of the low barriers on the out-of-plane deformation path. At the TD-CAM-B3LYP level, the TZP and DZP basis sets exhibit the barriers of less than 0.1 eV at $TS_{LE1\text{-}LE2}$ and $TS_{LE2\text{-}LE3}$. When the CC2 method is applied, the stationary-point energies are very similar to those of the TD-LC-BLYP-optimized structures for each of the TZVP and SV(P) basis sets. With respect to MIN_{LE3}, the S_1–S_0 energy gap is estimated to be about 0.8 eV at the TD-CAM-B3LYP level, while 0.6 eV at the CC2 level for the same structure.

The low barriers for the nonradiative decay of G are consistent with the extremely short excited-state lifetime of the GC pair in the gas phase, which was suggested by the observation of a broad band in the resonantly enhanced multiphoton ionization (REMPI) spectrum by Abo-Riziq et al.[17] The experimentally observed spectrum would correspond to the ionization from MIN_{LE1}. The REMPI spectrum for other minima such as MIN_{LE3} is less likely to be detected, because the FC factor should be very small owing to the largely out-of-plane deformed structure. The decay from MIN_{LE1} to S_1–S_0 CI is expected to take place very efficiently because the excited-state energies at $TS_{LE1\text{-}LE2}$ and $TS_{LE2\text{-}LE3}$ are definitely lower than the vertical excitation energy at the FC geometry, which agrees with the short lifetime of the excited state. Note that the deactivation with the EDPT mechanism is not ruled out by the present results. Rather it is likely to compete with the decay in the G moiety. The broad REMPI spectrum as well as the SPT reaction with the EDPT mechanism was reported to be unique to the Watson–Crick form,[7,17] suggesting a significant role of the latter in the excited-state dynamics. The presently calculated potential energy profiles of the EDPT process are discussed in Section 3.3.

To our knowledge, potential energy profiles for the decay of G in the GC pair were not reported in previous theoretical studies. This may be because out-of-plane deformation of hydrogen-bonded G in the

LE (G → G*) state was less taken into account in the calculation, where C_s symmetry was often assumed for the molecular structure of the GC pair.[5,7] Although a minimum of out-of-plane deformed structure corresponding to MIN_{LE1} was located in CIS calculations,[5] further out-of-plane deformation leading to the nonradiative decay was not considered. The decay in the G moiety was not observed even in on-the-fly molecular dynamics simulations of the photoexcited GC pair,[11,14,38] presumably because the CT (G → C*) state was initially populated rather than the LE (G → G*) state.

Another transition-state structure is located for the out-of-plane deformation of G. This transition state, labeled as $TS_{LE1\text{-}LE1}$, connects MIN_{LE1} and its mirror-image structure (referred to as MIN_{LE1}') via an IRC path. The TD-LC-BLYP/TZP energy of the $TS_{LE1\text{-}LE1}$ structure is 4.88 eV higher than the S_0 minimum energy and very similar to the energy of SP_{LE1}, see Fig. 1. The barrier height at $TS_{LE1\text{-}LE1}$ is calculated to be 0.17 eV from MIN_{LE1} (or MIN_{LE1}'). This barrier is in similar energy to the barrier for the nonradiative decay in G leading to MIN_{LE3}. Fig. 3 shows the TD-LC-BLYP/DZP potential energy curve along the IRC coordinate *s* for the inversion between MIN_{LE1} and MIN_{LE1}' through $TS_{LE1\text{-}LE1}$. The optimized structures of these stationary points (indicated by squares) are also shown in the figure. The potential energy curve is not symmetric with respect to $s = 0$, because the transition-state structure is non-planar. Note that there should be another IRC path starting with the mirror-image structure of $TS_{LE1\text{-}LE1}$, which is energetically identical to the IRC path shown in Fig. 3. Obviously there are the IRC paths for the nonradiative decay process from MIN_{LE1}' to the mirror-image structure of MIN_{LE3}.

3.3. Other reaction channels

This section discusses the potential energy profiles for photoreactions of the GC pair other than the decay in the G moiety. As shown in Fig. 1, the reaction path of SPT from G to C with the EDPT mechanism[5,7] exhibits a barrier on the potential energy curve in the S_1 state which lies in similar energy to the barriers for the decay in G. The transition-state structure is found to be completely planar in the TD-LC-BLYP/DZP geometry optimization with no symmetry constraint. The optimization with C_s symmetry constraint resulted in the same transition-state structure, which has only one imaginary-

frequency mode. This transition state is referred to as $TS_{LE1\text{-}CT1}$. The S_1 state at the $TS_{LE1\text{-}CT1}$ structure is characterized by the mixing of the configurations for the LE (G → G*) and CT (G → C*) excitations. The mixing of the LE and CT states at the transition state for SPT was also found in our recent LC-TDDFT study of the 7AI dimer.[45]

The energy of $TS_{LE1\text{-}CT1}$ is 4.99 eV higher than the S_0 minimum energy at the TD-LC-BLYP/TZP level. This transition state exhibits a barrier of 0.29 eV from MIN_{LE1}. Note that the energy of $TS_{LE1\text{-}CT1}$ is lower than the vertical excitation energy of the LE (G → G*) state (see Table 1). This result suggests that the SPT reaction path with the EDPT mechanism is energetically accessible with nearly planar molecular structures, that is, before the onset of out-of-plane deformation to reach a minimum in the LE state such as MIN_{LE1} or a crossing with the ground state. Thus, after UV absorption, this decay channel is likely to compete with the decay path for the out-of-plane deformation of G discussed in Section 3.2. In particular, the low barrier on the SPT path, which should be unique to the Watson–Crick form,[7] is expected to play an essential role for the broad REMPI spectrum of this form.[17]

The TD-LC-BLYP/DZP geometry optimization located a minimum of the CT (G → C*) state, labeled as MIN_{CT1}. At the optimized structure, the H atom attached to the N1 atom of G is transferred to the N atom of C along the NH…N hydrogen bond. This minimum also exhibits a non-planar structure due to a small pyramidalization at the amino group of C. Geometry optimization in C_s symmetry leads to a transition-state structure connecting MIN_{CT1} and its mirror-image structure (MIN_{CT1}') via an IRC path. This transition state is labeled as $TS_{CT1\text{-}CT1}$. The TD-LC-BLYP/TZP energies of MIN_{CT1} and $TS_{CT1\text{-}CT1}$ are 3.87 and 3.89 eV, respectively, higher than the S_0 minimum energy. Note that, in contrast to the case of the IRC path between MIN_{LE1} and MIN_{LE1}' (Fig. 3), there is only one IRC path connecting MIN_{CT1} and MIN_{CT1}' through $TS_{CT1\text{-}CT1}$ and that the potential energy curve along the path is symmetric with respect to $s = 0$.

Fig. 4 shows the potential energy curves in low-lying electronic states along the SPT reaction path. The IRC path in the S_1 state starting with $TS_{LE1\text{-}CT1}$ is determined at the TD-LC-BLYP/DZP level, while the electronic energies along the path are calculated with the (TD)DFT/DZP method using the LC-

BLYP, CAM-B3LYP and B3LYP functionals (Figs. 4a, b and c, respectively) as well as with the CC2/SV(P) method (Fig. 4d). The IRC path leads to stationary points of C_s structure in the LE (G → G*) and CT (G → C*) states, i.e. SP_{LE1} and $TS_{CT1\text{-}CT1}$, respectively. The geometry cannot be deviated from a planar one all along this IRC path, because the initial structure ($TS_{LE1\text{-}CT1}$) is in C_s symmetry and energy gradients with respect to the nuclear coordinates in the out-of-plane direction are always zero by the symmetry requirement. In the actual situation, however, the molecular system with kinetic energy should bifurcate to two product minima of C_1 symmetry (MIN_{CT1} and MIN_{CT1}') after passing a valley-ridge inflection (VRI) point between $TS_{LE1\text{-}CT1}$ and $TS_{CT1\text{-}CT1}$.[60,61]

The TD-LC-BLYP/DZP potential energy curves in Fig. 4a clearly show that the SPT reaction from G to C in the S_1 state is likely to occur with planar structure, accompanying the switch of electronic character from LE (G → G*) to CT (G → C*) (indicated by squares and triangles, respectively) along the IRC path. It should be noticed that the LE (G → G*) state is lower in energy than other excited states including the CT (G → C*) state at and near SP_{LE1} ($s < 0$ in Fig. 4a). This finding is consistent with the CC2 curves shown in Fig. 4d as well as with previous ab initio results.[7] At $TS_{LE1\text{-}CT1}$ ($s = 0$), the TD-LC-BLYP/DZP curve exhibits a barrier of 0.08 eV from SP_{LE1}. This small barrier for the LE-to-CT switching remains at the CC2/SV(P) level. As shown in Fig. 4d, the highest-energy point along the IRC path in the S_1 state is at $s = -0.35$ bohr·amu$^{1/2}$, where the barrier height from SP_{LE1} is estimated to be 0.04 eV. For the CT (G → C*) state, the TD-LC-BLYP method overestimates the excitation energy compared to the CC2 method. As a result, the $TS_{CT1\text{-}CT1}$ point in Fig. 4a exhibits an energy gap of 1.7 eV between the CT (G → C*) and S_0 states, which is larger than the gap of 1.0 eV in Fig 4d. Note that, however, this gap is likely to be compensated by additional in-plane motion (see the ESI for a representative result).

The TD-CAM-B3LYP calculation exhibits lower potential energies of the CT (G → C*) state than the TD-LC-BLYP calculation, see Fig 4b. This trend reflects the extent of long-range correction, as mentioned in Section 3.1. Thus the TD-CAM-B3LYP energies of the LE (G → G*) and CT (G → C*) states are very close to each other in the region near SP_{LE1} ($s < 0$ in Fig. 4b), resulting in significant

mixing of the LE and CT configurations. In particular, the barrier for the LE-to-CT switching disappears from the S_1 potential energy curve calculated with C_s symmetry at the TD-CAM-B3LYP level. With this respect, the present TD-LC-BLYP calculation exhibits more similar potential energy curves to the CC2 ones compared with the TD-CAM-B3LYP calculation. For the energy gap between the CT (G → C*) and S_0 states at $TS_{CT1\text{-}CT1}$, on the other hand, the TD-CAM-B3LYP method predicts closer value (0.7 eV) to the CC2 one than the TD-LC-BLYP method.

As shown in Fig. 4c, the B3LYP functional drastically underestimates the energy of the CT (G → C*) state as well as other CT states compared to the LC-BLYP and CAM-B3LYP functionals, which is expected for the conventional functional without LC. Even for the SP_{LE1} structure, the CT (G → C*) energy is lower by 1.4 eV than the LE (G → G*) energy at the TD-B3LYP/DZP level. This result strongly suggests that the long-range correction is required for a reliable description of the potential energy profiles of the EDPT reaction at the TDDFT level, which is critical to correctly predict the nonradiative decay mechanism in hydrogen-bonded base pairs.

Table 3 summarizes the energies of the barrier and minimum for the SPT reaction from G to C in the S_1 state calculated with the TDDFT and CC2 methods, which are relative to the S_0 minimum energy. For the barrier on the IRC path in Fig. 4, the TD-LC-BLYP method gives very similar energies of $TS_{LE1\text{-}CT1}$ with the TZP and DZP basis sets (4.99 and 5.03 eV, respectively), while the CC2 calculations at $s = -0.35$ bohr·amu$^{1/2}$ exhibit that the energy of the barrier differs by 0.3 eV between the TZVP and SV(P) basis sets (4.61 and 4.95 eV, respectively); see the upper half of Table 3. It is noteworthy that the energy of the barrier is a little higher than the transition-state energies for the out-of-plane deformation of G at each computational level, as shown in Tables 2 and 3. For MIN_{CT1}, the TD-LC-BLYP energy of the CT (G → C*) state is higher by about 1 eV than the CC2 energy. This result leads to the larger energy gap between the CT and S_0 states at the TD-LC-BLYP level, as shown in Fig. 4a.

Geometry optimization of the transition state for the LE-to-CT switching corresponding to $TS_{LE1\text{-}CT1}$ was also carried out with the TD-CAM-B3LYP/DZP method, resulting in a structure of C_1 symmetry. The TD-CAM-B3LYP and CC2 energies of the barrier calculated at the optimized structure are given in

the lower half of Table 3. The calculated energies tend to be lower than the energies of the barrier at the TD-LC-BLYP-optimized structure. However, these barriers are still in very similar energy to the barriers for the out-of-plane deformation of G (see also Table 2), suggesting that the decay in G and the SPT from G to C can compete in the GC pair. Table 3 also shows the energies the MIN_{CT1} structure optimized at the TD-CAM-B3LYP/DZP level, where the TD-CAM-B3LYP and CC2 methods give similar energies.

The energy diagram in Fig. 1 also suggests that the transition from the LE (G → G*) to LE (C → C*) state is likely to occur by overcoming a barrier with a similar height to that for the SPT reaction from G to C. The transition state for this process, denoted as $TS_{LE1\text{-}LE4}$, is found at a completely planar structure in C_s symmetry when optimized with the TD-LC-BLYP/DZP method. The energy of $TS_{LE1\text{-}LE4}$ is 5.02 eV higher than the S_0 minimum energy and the barrier height from MIN_{LE1} is 0.31 eV at the TD-LC-BLYP/TZP level. The IRC calculation from $TS_{LE1\text{-}LE4}$ leads to two stationary-point structures in C_s symmetry. One structure is SP_{LE1} in the LE (G → G*) state, while the other is a second-order saddle point in the LE (C → C*) state, labeled as SP_{LE4}. The LE (C → C*) state lies in the S_1 state at the SP_{LE4} structure. A transition-state structure is also found in this state, whose energy and structure are very similar to those of SP_{LE4}. This transition state in the LE (C → C*) state is denoted as $TS_{LE4\text{-}LE4}$, in analogy to $TS_{LE1\text{-}LE1}$ in the LE (G → G*) state.

Minimum in the LE (C → C*) state with molecular structure of C_1 symmetry could not be located by the TD-LC-BLYP/DZP geometry optimization in the S_1 state. Instead, the S_1–S_0 CI was encountered during the optimization by a large out-of-plane deformation of C. This result suggests that the nonradiative decay in C via the CI is likely to efficiently occur through a barrierless pathway once the LE (C → C*) is populated. This CI is also expected to be accessed by a relaxation from the S_2 to S_1 state after the LE (C → C*) excitation at the FC geometry.

Fig. 5 shows the TD-LC-BLYP/DZP potential energy curves along the IRC path in the LE (C → C*) state starting with the $TS_{LE4\text{-}LE4}$ structure (indicated by diamond). In both $s > 0$ and $s < 0$, the IRC calculation leads to a CI structure with the energy gradient of the LE (C → C*) state being far from zero.

No barrier was found between $TS_{LE4\text{-}LE4}$ and the CI structures, which is in agreement with previous ab initio results.[5] At the final point of the IRC calculation on each side (indicated by cross), the energy gap between the S_1 and S_0 states is less than 0.3 eV. The geometries at these points exhibit a ring puckering of C characterized by a significant twisting of the C=C double bond in the six-membered ring, which is known as the "ethylenic" reaction.[5,33-37] The two CI structures in $s > 0$ and $s < 0$ are almost (but not completely) the mirror image of each other. The potential energy curves along the IRC path are not perfectly symmetric with respect to $s = 0$, because $TS_{LE4\text{-}LE4}$ is slightly deviated from the planar structure.

The DPT reaction path in the LE (G → G*) state exhibits a higher barrier than the SPT reaction from G to C and nonradiative decay in each base, see Fig. 1. In the DPT reaction, one proton moves from the N1 atom of G to the N atom of C, and another moves from the N atom in the amino group of C to the O atom in the carbonyl group of G. The transition-state structure on the DPT path, referred to as $TS_{LE1\text{-}LE5}$, is located higher in energy by 5.25 eV than the FC geometry and by 0.55 eV than MIN_{LE1} at the TD-LC-BLYP/TZP level. The product minimum, labeled as MIN_{LE5}, is found at similar energy to $TS_{LE1\text{-}LE5}$ (5.18 eV relative to the S_0 minimum), suggesting a shallow minimum for the tautomer form. No minima for the intermediate of SPT structure were found in the LE (G → G*) state, suggesting that this reaction is likely to occur with the concerted mechanism rather than the stepwise mechanism. These findings are consistent with the ab initio results by Guallar et al.[10] The optimized structures of $TS_{LE1\text{-}LE5}$ and MIN_{LE5} are slightly deviated from C_s symmetry. The DPT reaction path in the LE (C → C*) could not be calculated in the present work, because the geometry optimization of this state resulted in the S_1–S_0 CI of the ethylenic structure.

Fig. 6 compares the potential energy profiles of low-lying electronic states along the DPT reaction path through $TS_{LE1\text{-}LE5}$, calculated with the (TD-)LC-BLYP, (TD-)CAM-B3LYP and (TD-)B3LYP methods using the DZP basis set and with the CC2 method using the SV(P) basis set. The IRC path in the LE (G → G*) state is determined at the TD-LC-BLYP/DZP level. As shown in Fig. 6a, the TD-LC-BLYP calculation predicts that the LE (G → G*) state (indicated by squares) remains to be S_1 along the reaction path and that no CT states lie below 6 eV (relative to the S_0 minimum). The TD-CAM-B3LYP

potential energy curves in Fig. 6b exhibit lower energy of the CT (G → C*) state (indicated by triangles) compared to the TD-LC-BLYP curves, but the LE (G → G*) state still lies in the S_1 state. For the TD-B3LYP curve in Fig. 6c, on the other hand, the energy of the CT (G → C*) state is significantly underestimated and thus lower than the energy of the LE (G → G*) state all along the IRC path. These results indicate that the long-range correction is critical also for correctly describing the potential energy curves of the excited-state DPT reaction, as has been reported for the 7AI dimer.[45] This conclusion for the GC pair is supported by the CC2/SV(P) curves in Fig. 6d, which exhibit intermediate results between the TD-LC-BLYP and TD-CAM-B3LYP curves for the CT (G → C*) state.

The minimum and transition state for the SPT reaction from C to G with the EDPT mechanism, labeled as MIN_{CT2} and $TS_{LE1\text{-}CT2}$, respectively, were also located by the TD-LC-BLYP/DZP geometry optimization; see Fig. 1. On the reaction path through $TS_{LE1\text{-}CT2}$, the proton transfer occurs from the amino group of C to the carbonyl group of G, accompanied by the charge-transfer excitation from a π orbital of C to a π* orbital of G, denoted as CT (C → G*). At the optimized structures of MIN_{CT2} and $TS_{LE1\text{-}CT2}$, the angle between the molecular planes of the two bases is considerably deviated from 180°. These structures also exhibit a significant rotation of the OH bond of G formed by the SPT and a pyramidalization of the amino group of G. The TD-LC-BLYP/TZP energies of these stationary points are much higher than the vertical excitation energies of the LE (G → G*) and LE (C → C*) states at the FC geometry, suggesting that this SPT reaction is not likely to be involved in the photophysics of the GC pair after the excitation to these states.

The present calculations have estimated the relative height of barriers on the potential energy curves for photoreaction channels of the GC pair. However, kinetic energy should be taken into account for the complete understanding of the accessibility of each channel in the excited-state dynamics. Some of the calculated barriers are very small and thus likely to be overcome if substantial kinetic energy has been gained. It is particularly expected that the SPT process from G to C can compete effectively with the out-of-plane deformation of G. As discussed above, the broad REMPI spectrum unique to the Watson–

Crick form[17] suggests a significant role of intermolecular proton transfer in the photoinduced dynamics of the GC pair in the gas phase.

Effects of biological environment would also be significant in the photoinduced processes of the DNA base pair. Interaction with polar solvent may considerably affect the energy of the CT state, as suggested in recent theoretical and experimental studies.[12,26] For the DNA double helix, spectroscopic studies have shown that base stacking can play an essential role in the excited-state dynamics.[62,63] One possible suggestion from the present results is that the decay mechanism of each base (in particular, guanine) may be available even in the biological relevant system with interbase hydrogen bonds if the effect of the base stacking and other environmental effects are small.

4. Conclusions

Potential energy profiles for the photoinduced processes in the Watson–Crick form of the GC base pair have been comprehensively examined with the LC-TDDFT method using the LC-BLYP and CAM-B3LYP functionals. For comparison, the ab initio CC2 method and the conventional TDDFT method with the B3LYP functional have also been employed. In the LC-TDDFT calculations, the reaction paths proposed in previous ab initio studies are qualitatively reproduced, and another path is found for nonradiative decay in G with hydrogen-bonded to C. The decay channel of G exhibits the barriers whose energies are definitely lower than the vertical excitation energies at the FC geometry, suggesting that this decay process is likely to be involved in the photoinduced dynamics of the hydrogen-bonded GC pair. This result is also supported by the CC2 calculations. A large out-of-plane deformation of the six-membered ring and amino group characterizing the nonradiative decay of isolated G is also observed in the decay path of hydrogen-bonded G.

The LC-TDDFT calculations also support that deactivation paths are likely to be open for previously proposed mechanisms including the SPT reaction from G to C and the decay in C. The photoinduced

mutation by the DPT reaction exhibits higher energy of the barrier than the SPT from G to C and the decay in each base. The reaction path for the SPT reaction from C to G has been found, but this channel is not likely to be involved in the photophysics of the GC pair because of very high potential energy. With respect to the excited-state SPT and DPT reactions, it has been exhibited that the long-range correction to TDDFT is critical for a correct prediction of potential energy profiles.

The present computational results suggest that nonradiative decay in individual bases and the EDPT reaction between the bases can compete in hydrogen-bonded DNA base pairs and play a significant role in the mechanism of photostability. It is interesting that the photostability seems to be supported by many competing mechanisms of ultrafast nonradiative deactivation. For the full understanding of the photophysics of base pairs, further theoretical studies on the dynamics in the excited state and the effects of biological environment would be necessary.

Acknowledgements

This work has been supported by a Grant-in-Aid for Scientific Research from the Ministry of Education, Culture, Sports, Science and Technology (MEXT), Japan. S.Y. thanks the Japan Society for the Promotion of Science (JSPS) for the Research Fellowships for Young Scientists. The authors acknowledge substantial allocation of computing time by the Research Center for Computational Science (RCCS), Okazaki, Japan.

References

1. C. E. Crespo-Hernández, B. Cohen, P. M. Hare and B. Kohler, *Chem. Rev.*, 2004, **104**, 1977–2019.
2. M. Shukla and J. Leszczynski, eds., *Radiation Induced Molecular Phenomena in Nucleic Acids: A Comprehensive Theoretical and Experimental Analysis*, Springer, Berlin, 2008.
3. W. Domcke, D. R. Yarkony and H. Köppel, eds., *Conical Intersections: Electronic Structure, Dynamics and Spectroscopy*, World Scientific, Singapore, 2004.
4. A. L. Sobolewski and W. Domcke, *Chem. Phys.*, 2003, **294**, 73–83.
5. A. L. Sobolewski and W. Domcke, *Phys. Chem. Chem. Phys.*, 2004, **6**, 2763–2771.
6. T. Schultz, E. Samoylova, W. Radloff, I. V. Hertel, A. L. Sobolewski and W. Domcke, *Science*, 2004, **306**, 1765–1768.
7. A. L. Sobolewski, W. Domcke and C. Hättig, *Proc. Natl. Acad. Sci. U.S.A.*, 2005, **102**, 17903–17906.
8. S. Perun, A. L. Sobolewski and W. Domcke, *J. Phys. Chem. A*, 2006, **110**, 9031–9038.
9. P.-O. Löwdin, *Rev. Mod. Phys.*, 1963, **35**, 724–732.
10. V. Guallar, A. Douhal, M. Moreno and J. M. Lluch, *J. Phys. Chem. A*, 1999, **103**, 6251–6256.
11. G. Groenhof, L. V. Schäfer, M. Boggio-Pasqua, M. Goette, H. Grubmüller and M. A. Robb, *J. Am. Chem. Soc.*, 2007, **129**, 6812–6819.
12. F. Santoro, V. Barone and R. Improta, *J. Am. Chem. Soc.*, 2009, **131**, 15232–15245.
13. I. Conti, P. Altoe, M. Stenta, M. Garavelli and G. Orlandi, *Phys. Chem. Chem. Phys.*, 2010, **12**, 5016–5023.
14. A. N. Alexandrova, J. C. Tully and G. Granucci, *J. Phys. Chem. B*, 2010, **114**, 12116–12128.
15. Y. Lu, Z. Lan and W. Thiel, *Angew. Chem., Int. Ed.*, 2011, **50**, 6864–6867.
16. E. Samoylova, H. Lippert, S. Ullrich, I. V. Hertel, W. Radloff and T. Schultz, *J. Am. Chem. Soc.*, 2005, **127**, 1782–1786.
17. A. Abo-Riziq, L. Grace, E. Nir, M. Kabelac, P. Hobza and M. S. de Vries, *Proc. Natl. Acad. Sci. U. S. A.*, 2005, **102**, 20–23.
18. N. K. Schwalb and F. Temps, *J. Am. Chem. Soc.*, 2007, **129**, 9272–9273.
19. N. Gador, E. Samoylova, V. R. Smith, A. Stolow, D. M. Rayner, W. G. Radloff, I. V. Hertel and T. Schultz, *J. Phys. Chem. A*, 2007, **111**, 11743–11749.
20. F.-A. Miannay, A. Banyasz, T. Gustavsson and D. Markovitsi, *J. Am. Chem. Soc.*, 2007, **129**, 14574–14575.

21. E. Samoylova, T. Schultz, I. V. Hertel and W. Radloff, *Chem. Phys.*, 2008, **347**, 376–382.
22. C. E. Crespo-Hernández, K. de La Harpe and B. Kohler, *J. Am. Chem. Soc.*, 2008, **130**, 10844–10845.
23. K. de La Harpe, C. E. Crespo-Hernández and B. Kohler, *J. Am. Chem. Soc.*, 2009, **131**, 17557–17559.
24. N. K. Schwalb, T. Michalak and F. Temps, *J. Phys. Chem. B*, 2009, **113**, 16365–16376.
25. I. Vayá, P. Changenet-Barret, T. Gustavsson, D. Zikich, A. B. Kotlyar and D. Markovitsi, *Photochem. Photobiol. Sci.*, 2010, **9**, 1193–1195.
26. L. Biemann, S. A. Kovalenko, K. Kleinermanns, R. Mahrwald, M. Markert and R. Improta, *J. Am. Chem. Soc.*, 2011, **133**, 19664–19667.
27. H. Chen and S. Li, *J. Chem. Phys.*, 2006, **124**, 154315.
28. C. M. Marian, *J. Phys. Chem. A*, 2007, **111**, 1545–1553.
29. L. Serrano-Andrés, M. Merchán and A. C. Borin, *J. Am. Chem. Soc.*, 2008, **130**, 2473–2484.
30. S. Yamazaki, W. Domcke and A. L. Sobolewski, *J. Phys. Chem. A*, 2008, **112**, 11965–11968.
31. N. Ismail, L. Blancafort, M. Olivucci, B. Kohler and M. A. Robb, *J. Am. Chem. Soc.*, 2002, **124**, 6818–6819.
32. M. Merchán and L. Serrano-Andrés, *J. Am. Chem. Soc.*, 2003, **125**, 8108–8109.
33. M. Z. Zgierski, S. Patchkovskii and E. C. Lim, *J. Chem. Phys.*, 2005, **123**, 081101.
34. K. Tomić, J. Tatchen and C. M. Marian, *J. Phys. Chem. A*, 2005, **109**, 8410–8418.
35. M. Merchán, R. González-Luque, T. Climent, L. Serrano-Andrés, E. Rodríguez, M. Reguero and D. Peláez, *J. Phys. Chem. B* 2006, **110**, 26471–26476.
36. L. Blancafort, *Photochem. Photobiol.*, 2007, **83**, 603–610.
37. K. A. Kistler and S. Matsika, *J. Phys. Chem. A*, 2007, **111**, 2650–2661.
38. P. R. L. Markwick and N. L. Doltsinis, *J. Chem. Phys.*, 2007, **126**, 175102.
39. Y. Tawada, T. Tsuneda, S. Yanagisawa, T. Yanai and K. Hirao, *J. Chem. Phys.*, 2004, **120**, 8425–8433.
40. M. Chiba, T. Tsuneda and K. Hirao, *J. Chem. Phys.*, 2006, **124**, 144106.
41. A. Dreuw, J. L. Weisman and M. Head-Gordon, *J. Chem. Phys.*, 2003, **119**, 2943–2946.
42. A. W. Lange and J. M. Herbert, *J. Am. Chem. Soc.*, 2009, **131**, 3913–3922.
43. L. Jensen and N. Govind, *J. Phys. Chem. A*, 2009, **113**, 9761–9765.
44. M. K. Shukla and J. Leszczynski, *Mol. Phys.*, 2010, **108**, 3131–3146.
45. X. Yu, S. Yamazaki and T. Taketsugu, *J. Chem. Theory Comput.*, 2011, **7**, 1006–1015.
46. O. Christiansen, H. Koch and P. Jørgensen, *Chem. Phys. Lett.*, 1995, **243**, 409–418.
47. A. D. Becke, *Phys. Rev. A*, 1988, **38**, 3098–3100.

48. C. Lee, W. Yang and R. G. Parr, *Phys. Rev. B*, 1988, **37**, 785–789.
49. T. Yanai, D. P. Tew and N. C. Handy, *Chem. Phys. Lett.*, 2004, **393**, 51–57.
50. A. D. Becke, *J. Chem. Phys.*, 1993, **98**, 5648–5652.
51. P. J. Stephens, F. J. Devlin, C. F. Chabalowski and M. J. Frisch, *J. Phys. Chem.*, 1994, **98**, 11623–11627.
52. T. Noro, M. Sekiya, Y. Osanai, E. Miyoshi, T. Koga and H. Tatewaki, *Segmented Gaussian Basis Set*, http://setani.sci.hokudai.ac.jp/sapporo/.
53. M. W. Schmidt, K. K. Baldridge, J. A. Boatz, S. T. Elbert, M. S. Gordon, J. H. Jensen, S. Koseki, N. Matsunaga, K. A. Nguyen, S. Su, T. L. Windus, M. Dupuis and J. A. Montgomery, Jr., *J. Comput. Chem.*, 1993, **14**, 1347–1363.
54. C. Hättig and F. Weigend, *J. Chem. Phys.*, 2000, **113**, 5154–5161.
55. A. Schäfer, H. Horn and R. Ahlrichs, *J. Chem. Phys.*, 1992, **97**, 2571–2577.
56. A. Schäfer, C. Huber and R. Ahlrichs, *J. Chem. Phys.*, 1994, **100**, 5829–5835.
57. F. Weigend and R. Ahlrichs, *Phys. Chem. Chem. Phys.*, 2005, **7**, 3297–3305.
58. R. Ahlrichs, M. Bär, M. Häser, H. Horn and C. Kölmel, *Chem. Phys. Lett.*, 1989, **162**, 165–169.
59. M. P. Fülscher, L. Serrano-Andrés and B. O. Roos, *J. Am. Chem. Soc.*, 1997, **119**, 6168–6176.
60. P. Valtazanos and K. Ruedenberg, *Theor. Chim. Acta*, 1986, **69**, 281–307.
61. T. Yanai, T. Taketsugu, and K. Hirao, *J. Chem. Phys.*, 1997, **107**, 1137–1146.
62. C. E. Crespo-Hernández, B. Cohen and B. Kohler, *Nature*, 2005, **436**, 1141–1144.
63. N. K. Schwalb and F. Temps, *Science*, 2008, **322**, 243–245.

Figure Captions

Fig. 1 Energy diagram for photoinduced processes in GC pair. TD-LC-BLYP/TZP energies are shown for Franck–Condon (FC) geometry as well as excited-state stationary points including minimum (MIN), transition state (TS), and second-order saddle point (SP). These geometries are optimized at the (TD-)LC-BLYP/DZP level. The excited-state energies are relative to the ground-state energy of the FC geometry. Optimized structures of some stationary points are also shown. Stationary points indicated by (C_s) are in a planar structure of C_s symmetry, while the other stationary points are in C_1 structure.

Fig. 2 Excited-state stationary-point structures of GC pair relevant to out-of-plane deformation of the G moiety, optimized at the TD-LC-BLYP/DZP level: (a) MIN_{LE1}, (b) $TS_{LE1\text{-}LE2}$, (c) MIN_{LE2}, (d) $TS_{LE2\text{-}LE3}$ and (e) MIN_{LE3}. Bond lengths are given in Å.

Fig. 3 (TD-)LC-BLYP/DZP potential energy curves in the S_0 and LE ($G \rightarrow G^*$) states along the IRC coordinate *s* starting with $TS_{LE1\text{-}LE1}$ structure. Energies are relative to the ground-state energy of the FC geometry. $TS_{LE1\text{-}LE1}$, MIN_{LE1} and its mirror-image structure (MIN_{LE1}') on the IRC path are indicated by squares, and optimized structures of these stationary points are also shown.

Fig. 4 Potential energy curves in the ground state and low-lying excited states along the SPT reaction path through $TS_{LE1\text{-}CT1}$ as a function of the IRC coordinate *s*. The IRC path is determined at the TD-LC-BLYP/DZP level, while electronic energies along the path are calculated with the (TD)DFT/DZP method using the (a) LC-BLYP, (b) CAM-B3LYP and (c) B3LYP functionals and the (d) CC2 method with the SV(P) basis set. Square and triangle indicate the energy of the lowest LE ($G \rightarrow G^*$) and CT ($G \rightarrow C^*$) states, respectively. Energies are relative to the ground-state energy of the FC geometry. Optimized structures of relevant stationary points are also shown.

Fig. 5 (TD-)LC-BLYP/DZP potential energy curves in the S_0 and LE (C → C*) states along the IRC coordinate *s* starting with $TS_{LE4\text{-}LE4}$ structure. Energies are relative to the ground-state energy of the FC geometry. $TS_{LE4\text{-}LE4}$ on the path ($s = 0$) is indicated by diamond, while the final point of the IRC calculation on each side ($s = 5.69$ and -5.41 bohr·amu$^{1/2}$) is indicated by cross. Structures of the transition state and final points are also shown.

Fig. 6 Potential energy curves in the ground state and low-lying excited states along the DPT reaction path from MIN_{LE1} to MIN_{LE5} through $TS_{LE1\text{-}LE5}$ as a function of the IRC coordinate *s*. The IRC path is determined at the TD-LC-BLYP/DZP level, while electronic energies along the path are calculated with the (TD)DFT/DZP method using the (a) LC-BLYP, (b) CAM-B3LYP and (c) B3LYP functionals and the (d) CC2 method with the SV(P) basis set. Square and triangle indicate the energy of the lowest LE (G → G*) and CT (G → C*) states, respectively. Energies are relative to the ground-state energy of the FC geometry. Optimized structures of relevant stationary points are also shown.

Table 1 TDDFT/TZP and CC2/TZVP vertical excitation energies (ΔE, eV) and oscillator strengths (f, in parentheses) for low-lying singlet excited states of GC pair and isolated G and C monomers at the ground-state equilibrium geometry optimized with the LC-BLYP/DZP method.

	LC-BLYP/TZP		CAM-B3LYP/TZP		B3LYP/TZP		CC2/TZVP	
State	ΔE, f	Transition	ΔE, f	Transition	ΔE, f	Transition	ΔE, f	Transition
GC pair								
S_1	5.09 (0.080)	$^1\pi\pi^*$ (G → G*)	4.93 (0.037)	$^1\pi\pi^*$ (G → C*)	3.39 (0.002)	$^1\pi\pi^*$ (G → C*)	4.88 (0.061)	$^1\pi\pi^*$ (G → G*)
S_2	5.27 (0.113)	$^1\pi\pi^*$ (C → C*)	5.21 (0.061)	$^1\pi\pi^*$ (G → G*)	4.67 (0.009)	$^1\pi\pi^*$ (G → C*)	5.06 (0.063)	$^1\pi\pi^*$ (C → C*)
S_3	5.68 (0.465)	$^1\pi\pi^*$ (G → G*)	5.29 (0.100)	$^1\pi\pi^*$ (C → C*)	4.82 (0.000)	$^1n\pi^*$ (G → C*)	5.23 (0.028)	$^1\pi\pi^*$ (G → C*)
S_4	5.73 (0.001)	$^1n\pi^*$ (C → C*)	5.61 (0.416)	$^1\pi\pi^*$ (G → G*)	4.85 (0.096)	$^1\pi\pi^*$ (G → G*)	5.49 (0.001)	$^1n\pi^*$ (C → C*)
S_5	5.88 (0.107)	$^1\pi\pi^*$ (C → C*)	5.71 (0.001)	$^1n\pi^*$ (C → C*)	4.89 (0.000)	$^1\pi\sigma^*$ (G → C*)	5.50 (0.183)	$^1\pi\pi^*$ (C → C*)
S_6	5.91 (0.000)	$^1n\pi^*$ (G → G*)	5.80 (0.100)	$^1\pi\pi^*$ (C → C*)	4.95 (0.034)	$^1\pi\pi^*$ (C → C*)	5.51 (0.425)	$^1\pi\pi^*$ (G → G*)
S_7	6.00 (0.008)	$^1\pi\pi^*$ (G → C*)	5.96 (0.000)	$^1n\pi^*$ (G → G*)	5.14 (0.041)	$^1\pi\pi^*$ (GC → C*) [a]	5.80 (0.000)	$^1n\pi^*$ (C → C*)
S_8	6.17 (0.000)	$^1\pi\sigma^*$ (G → G*)	5.98 (0.000)	$^1\pi\sigma^*$ (G → G*)	5.18 (0.000)	$^1n\pi^*$ (G → C*)	5.90 (0.000)	$^1n\pi^*$ (G → G*)
S_9	6.29 (0.002)	$^1n\pi^*$ (G → G*)	6.25 (0.003)	$^1\pi\pi^*$ (G → C*)	5.29 (0.264)	$^1\pi\pi^*$ (G → G*)	6.24 (0.000)	$^1\pi\sigma^*$ (G → G*)
S_{10}	6.44 (0.000)	$^1n\pi^*$ (C → C*)	6.32 (0.002)	$^1n\pi^*$ (G → G*)	5.35 (0.000)	$^1\pi\sigma^*$ (G → G*)	6.30 (0.001)	$^1n\pi^*$ (G → G*)
G monomer								
S_1	5.25 (0.143)	$^1\pi\pi^*$ (G → G*)	5.25 (0.142)	$^1\pi\pi^*$ (G → G*)	4.89 (0.001)	$^1\pi\sigma^*$ (G → G*)	5.20 (0.160)	$^1\pi\pi^*$ (G → G*)
S_2	5.57 (0.000)	$^1n\pi^*$ (G → G*)	5.62 (0.002)	$^1\pi\sigma^*$ (G → G*)	5.02 (0.114)	$^1\pi\pi^*$ (G → G*)	5.64 (0.000)	$^1n\pi^*$ (G → G*)
S_3	5.79 (0.352)	$^1\pi\pi^*$ (G → G*)	5.64 (0.000)	$^1n\pi^*$ (G → G*)	5.32 (0.254)	$^1\pi\pi^*$ (G → G*)	5.66 (0.335)	$^1\pi\pi^*$ (G → G*)
S_4	5.85 (0.002)	$^1\pi\sigma^*$ (G → G*)	5.70 (0.328)	$^1\pi\pi^*$ (G → G*)	5.39 (0.000)	$^1n\pi^*$ (G → G*)	5.87 (0.002)	$^1\pi\sigma^*$ (G → G*)
C monomer								
S_1	5.05 (0.069)	$^1\pi\pi^*$ (C → C*)	5.05 (0.064)	$^1\pi\pi^*$ (C → C*)	4.73 (0.037)	$^1\pi\pi^*$ (C → C*)	4.85 (0.052)	$^1\pi\pi^*$ (C → C*)
S_2	5.31 (0.001)	$^1n\pi^*$ (C → C*)	5.35 (0.001)	$^1n\pi^*$ (C → C*)	4.84 (0.000)	$^1n\pi^*$ (C → C*)	5.08 (0.001)	$^1n\pi^*$ (C → C*)
S_3	5.98 (0.000)	$^1n\pi^*$ (C → C*)	6.00 (0.000)	$^1n\pi^*$ (C → C*)	5.22 (0.001)	$^1n\pi^*$ (C → C*)	5.49 (0.001)	$^1n\pi^*$ (C → C*)
S_4	6.08 (0.142)	$^1\pi\pi^*$ (C → C*)	6.01 (0.120)	$^1\pi\pi^*$ (C → C*)	5.52 (0.081)	$^1\pi\pi^*$ (C → C*)	5.77 (0.151)	$^1\pi\pi^*$ (C → C*)

[a] π orbital is delocalized on the G and C moieties.

Table 2 TDDFT and CC2 energies (eV) of stationary-point structures in the S_1 state for out-of-plane deformation of the G moiety in GC pair. The energies are relative to the S_0 minimum energy.

Method	MIN_{LE1}	$TS_{LE1-LE2}$	MIN_{LE2}	$TS_{LE2-LE3}$	MIN_{LE3}
TD-LC-BLYP/DZP-optimized structures					
TD-LC-BLYP/TZP	4.70	4.81	4.80	4.87	4.58
TD-LC-BLYP/DZP	4.78	4.84	4.82	4.85	4.52
CC2/TZVP	4.37	4.42 [a]	4.26	4.36	3.90
CC2/SV(P)	4.55	4.63 [a]	4.39	4.46	3.94
TD-CAM-B3LYP/DZP-optimized structures					
TD-CAM-B3LYP/TZP	4.67	4.71	4.68	4.75	4.47
TD-CAM-B3LYP/DZP	4.77	4.79	4.72	4.75	4.42
CC2/TZVP	4.35	4.39	4.22	4.32	3.85
CC2/SV(P)	4.53	4.59	4.36	4.43	3.91

[a] At the point with the highest CC2/SV(P) energy on the IRC path between MIN_{LE1} and $TS_{LE1-LE2}$.

Table 3 TDDFT and CC2 energies (eV) of stationary-point structures in the S_1 state for SPT reaction from G to C. The energies are relative to the S_0 minimum energy.

Method	$TS_{LE1-CT1}$	MIN_{CT1}
TD-LC-BLYP/DZP-optimized structures		
TD-LC-BLYP/TZP	4.99	3.87
TD-LC-BLYP/DZP	5.03	3.78
CC2/TZVP	4.61 [a]	2.65
CC2/SV(P)	4.95 [a]	2.82
TD-CAM-B3LYP/DZP-optimized structures		
TD-CAM-B3LYP/TZP	4.72	2.76
TD-CAM-B3LYP/DZP	4.82	2.69
CC2/TZVP	4.43	2.64
CC2/SV(P)	4.67	2.80

[a] At the point with the highest CC2/SV(P) energy on the IRC path between SP_{LE1} and $TS_{LE1-CT1}$.

Figure 1

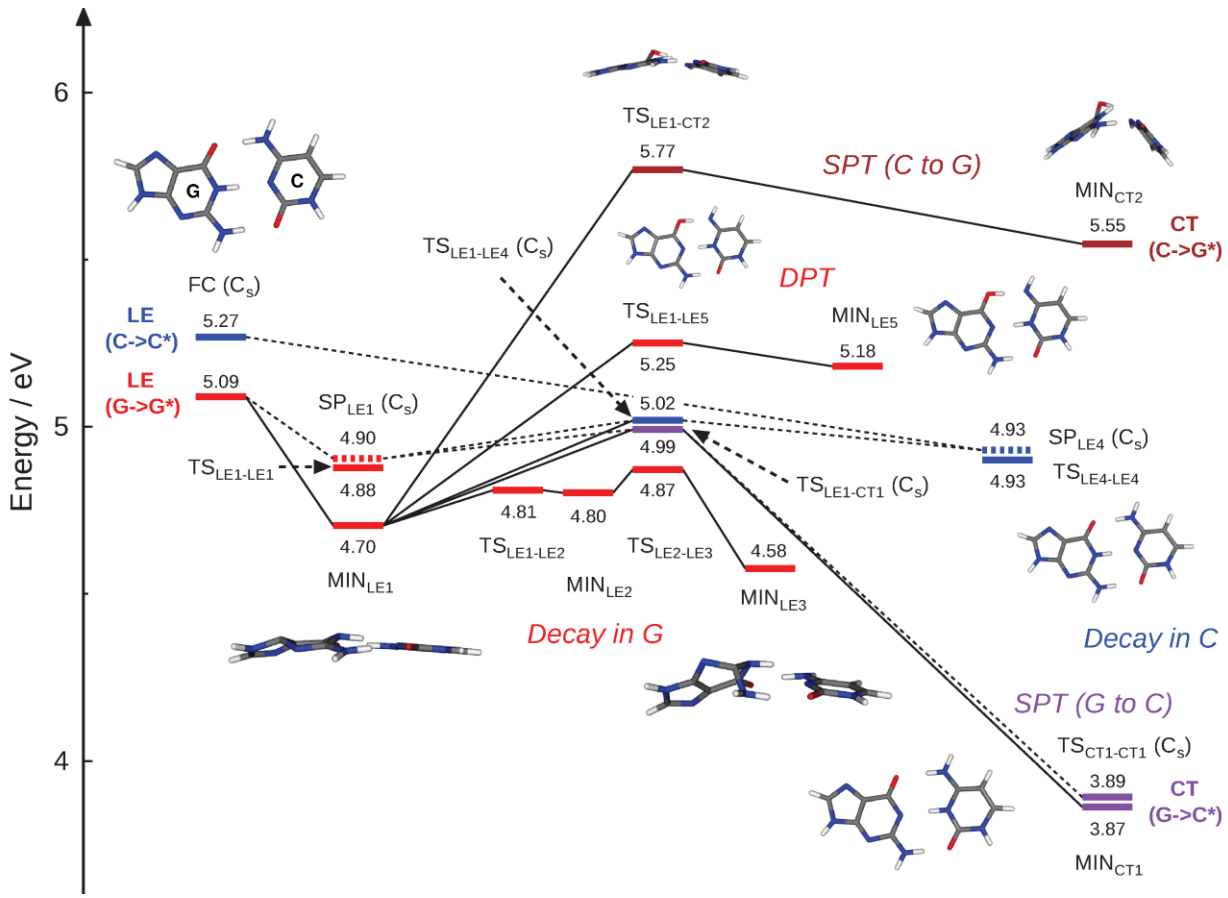
Energy / eV
6
5
4
G
C
FC (Cs)
LE
(C->C*)
5.27
LE
(G->G*)
5.09
SPLE1 (Cs)
4.90
TSLE1-LE1
4.88
4.70
MINLE1
TSLE1-LE4 (Cs)
TSLE1-CT2
5.77
SPT (C to G)
MINCT2
5.55
CT
(C->G*)
DPT
TSLE1-LE5
5.25
MINLE5
5.18
5.02
4.99
TSLE1-CT1 (Cs)
4.93
SPLE4 (Cs)
4.93
TSLE4-LE4
4.81
4.80
TSLE1-LE2
4.87
TSLE2-LE3
4.58
MINLE2
MINLE3
Decay in G
Decay in C
SPT (G to C)
TSCT1-CT1 (Cs)
3.89
CT
(G->C*)
3.87
MINCT1

Figure 2

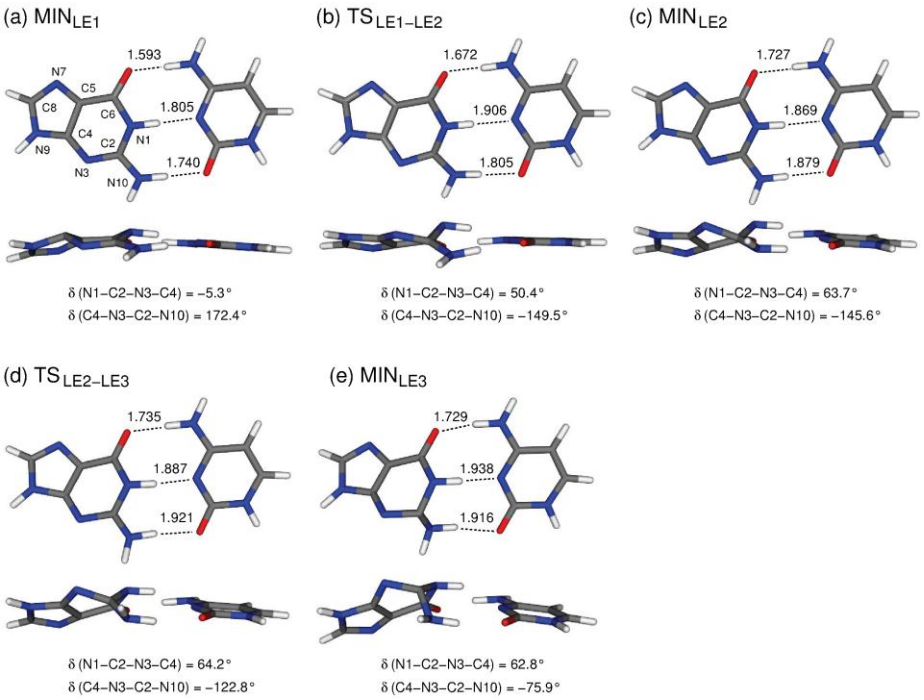
(a) MIN$_{LE1}$
1.593
1.805
1.740
N7
C5
C8
C6
C4
C2
N1
N9
N3
N10
δ (N1–C2–N3–C4) = –5.3°
δ (C4–N3–C2–N10) = 172.4°
(b) TS$_{LE1–LE2}$
1.672
1.906
1.805
δ (N1–C2–N3–C4) = 50.4°
δ (C4–N3–C2–N10) = –149.5°
(c) MIN$_{LE2}$
1.727
1.869
1.879
δ (N1–C2–N3–C4) = 63.7°
δ (C4–N3–C2–N10) = –145.6°
(d) TS$_{LE2–LE3}$
1.735
1.887
1.921
δ (N1–C2–N3–C4) = 64.2°
δ (C4–N3–C2–N10) = –122.8°
(e) MIN$_{LE3}$
1.729
1.938
1.916
δ (N1–C2–N3–C4) = 62.8°
δ (C4–N3–C2–N10) = –75.9°

Figure 3

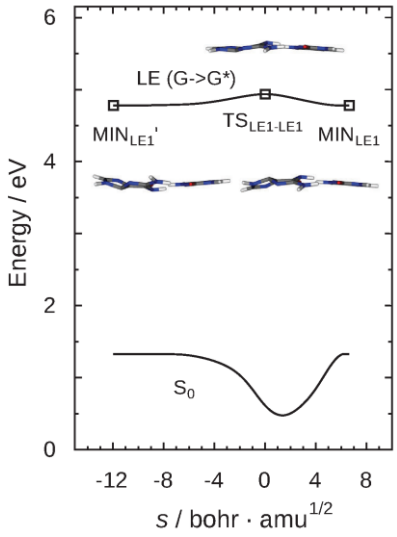
6
4
2
0
Energy / eV
LE (G->G*)
MIN$_{LE1}$'
TS$_{LE1-LE1}$
MIN$_{LE1}$
S$_0$
-12
-8
-4
0
4
8
s / bohr · amu$^{1/2}$

Figure 4

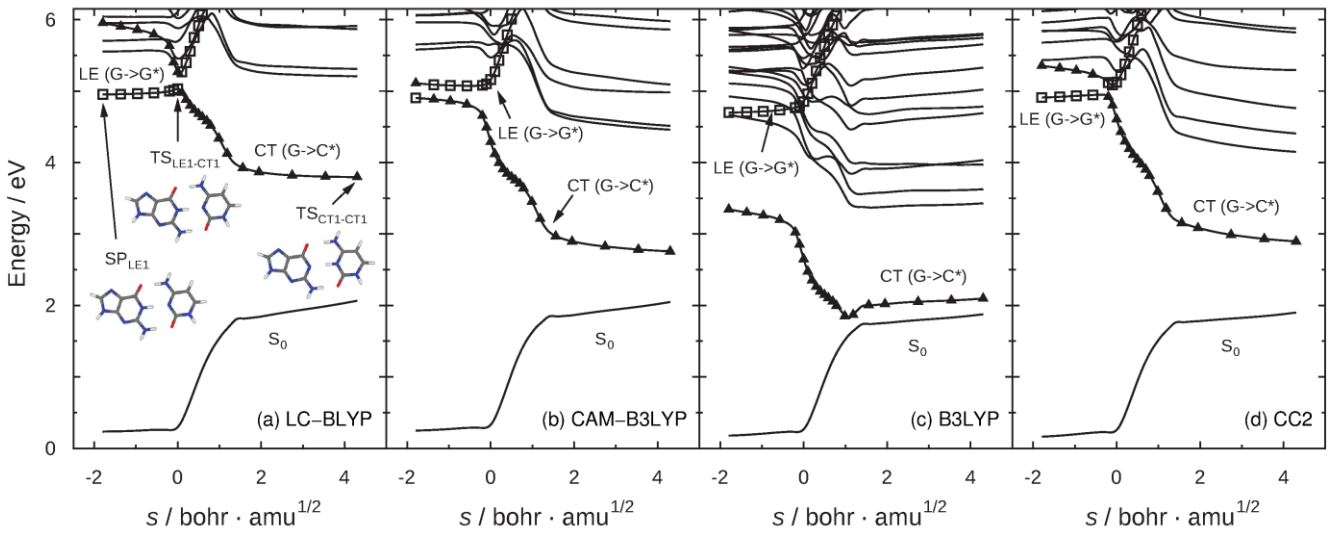
Energy / eV
LE (G->G*)
TS$_{LE1-CT1}$
CT (G->C*)
TS$_{CT1-CT1}$
SP$_{LE1}$
S$_0$
(a) LC–BLYP
(b) CAM–B3LYP
(c) B3LYP
(d) CC2
s / bohr · amu$^{1/2}$

Figure 5

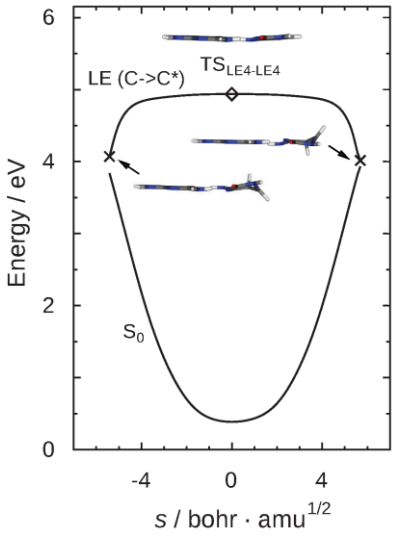

Figure 6

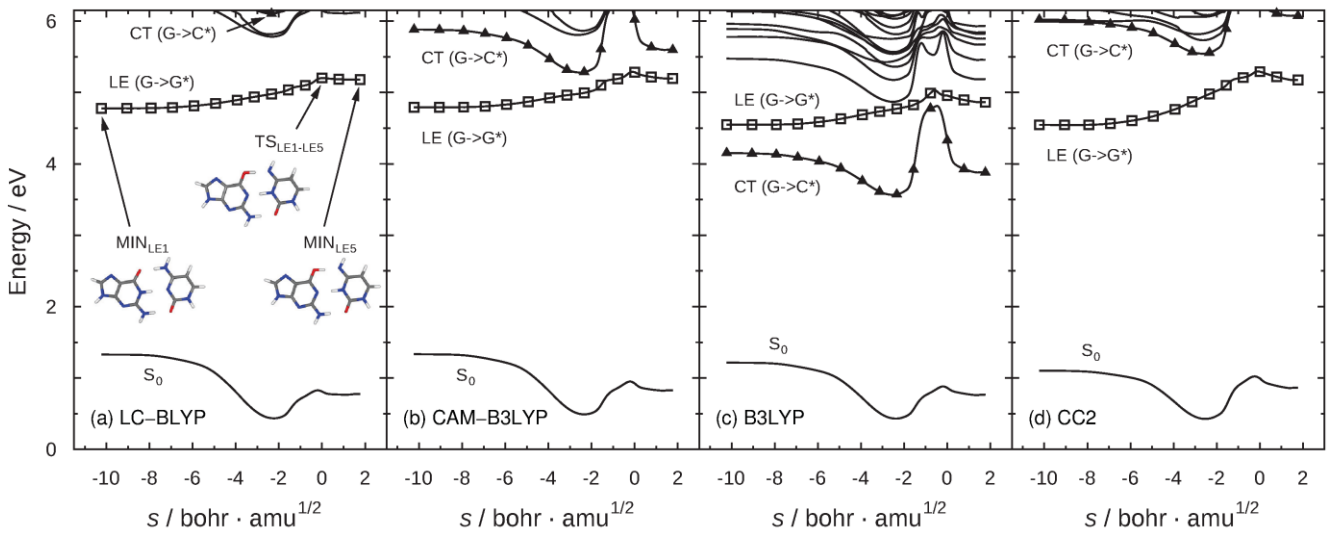
Energy / eV
CT (G->C*)
LE (G->G*)
TS$_{LE1-LE5}$
MIN$_{LE1}$
MIN$_{LE5}$
S$_0$
(a) LC–BLYP
(b) CAM–B3LYP
(c) B3LYP
(d) CC2
s / bohr · amu$^{1/2}$